Channel Estimation and Multipath Diversity Reception for RIS-Empowered Broadband Wireless Systems Based on Cyclic-Prefixed Single-Carrier Transmission

Qiang Li, *Member, IEEE*, Miaowen Wen, *Senior Member, IEEE*, Ertugrul Basar, *Fellow, IEEE*, George C. Alexandropoulos, *Senior Member, IEEE*, Kyeong Jin Kim, *Senior Member, IEEE*, and H. Vincent Poor, *Life Fellow, IEEE*

***Abstract*— In this paper, a cyclic-prefixed single-carrier (CPSC) transmission scheme with phase shift keying (PSK) signaling is presented for broadband wireless communications systems empowered by a reconfigurable intelligent surface (RIS). In the proposed CPSC-RIS, the RIS is configured according to the transmitted PSK symbols such that different cyclically delayed versions of the incident signal are created by the RIS to achieve multipath diversity. A practical and efficient channel estimator is developed for CPSC-RIS and the mean square error of the channel estimation is expressed in closed-form. We analyze the bit error rate (BER) performance of CPSC-RIS over frequency-selective Nakagami-m fading channels. An upper bound on the BER is derived by assuming maximum-likelihood detection. Furthermore, by applying the concept of index modulation (IM), we propose an extension of CPSC-RIS, termed CPSC-RIS-IM, which enhances the spectral efficiency. In addition to conventional constellation information of PSK symbols, CPSC-RIS-IM uses the full permutations of cyclic delays caused by the RIS to carry information. A sub-optimal receiver is designed for CPSC-RIS-IM to aim at low computational complexity. Our simulation results in terms of BER corroborate the performance analysis and the superiority of CPSC-RIS(-IM) over the conventional CPSC without an RIS and orthogonal frequency division multiplexing with an RIS.**

***Index Terms*— Channel estimation, cyclic delay diversity, cyclic-prefixed single-carrier, index modulation, reconfigurable intelligence surface.**

Manuscript received 5 January 2022; revised 25 June 2022 and 3 November 2022; accepted 18 December 2022. Date of publication 4 January 2023; date of current version 14 August 2023. This work was supported in part by the National Natural Science Foundation of China under Grant 62201228 and Grant 61871190, in part by the Guangdong Basic and Applied Basic Research Foundation under Grant 2020A1515110470 and Grant 2021B1515120067, in part by the Scientific and Technological Research Council of Turkey (TUBITAK) under Grant 120E401, in part by the European Union Horizon 2020 RISE-6G Project under Grant 101017011, and in part by the U.S. National Science Foundation under Grant CCF-1908308 and Grant CNS-2128448. An earlier version of this paper was presented in part at the EuCNC & 6G Summit 2022 [DOI: 10.1109/EuCNC/6GSummit54941.2022.9815627]. The associate editor coordinating the review of this article and approving it for publication was D. So. *(Corresponding author: Miaowen Wen.)*

Qiang Li is with the College of Information Science and Technology, Jinan University, Guangzhou 510632, China (e-mail: qiangli@jnu.edu.cn).

Miaowen Wen is with the School of Electronic and Information Engineering, South China University of Technology, Guangzhou 510640, China (e-mail: eemwwen@scut.edu.cn).

Ertugrul Basar is with the Department of Electrical and Electronics Engineering, Koç University, 34450 Istanbul, Turkey (e-mail: ebasar@ku.edu.tr).

George C. Alexandropoulos is with the Department of Informatics and Telecommunications, National and Kapodistrian University of Athens, 15784 Athens, Greece, and also with the Technology Innovation Institute, Masdar City, Abu Dhabi, United Arab Emirates (e-mail: alexandg@di.uoa.gr).

Kyeong Jin Kim is with the Mitsubishi Electric Research Laboratories, Cambridge, MA 02139 USA (e-mail: kkim@merl.com).

H. Vincent Poor is with the Department of Electrical and Computer Engineering, Princeton University, Princeton, NJ 08544 USA (e-mail: poor@princeton.edu).

Color versions of one or more figures in this article are available at https://doi.org/10.1109/TWC.2022.3232072.

Digital Object Identifier 10.1109/TWC.2022.3232072

I. Introduction

As an alternative to orthogonal frequency division multiplexing (OFDM), cyclic-prefixed single-carrier (CPSC) shares some OFDM advantages, such as low-complexity implementation, while avoiding several OFDM drawbacks, such as a high peak-to-average power ratio and high sensitivity to carrier frequency offsets [2], [3]. Moreover, uncoded CPSC with a minimum mean square error (MMSE) receiver is able to extract multipath diversity in frequency-selective fading channels for reasonably large values of block sizes and practical values of bit error rate (BER) [4], and multipath diversity in identical [5] and non-identical frequency selective fading channels [6] can be achieved by a maximum-likelihood (ML) receiver irrespective of the uncoded block size. By contrast, without channel coding or precoding techniques, OFDM cannot harvest any multipath diversity even with the optimal ML receiver [4]. CPSC is a promising solution to broadband wireless communications, and has been included in the 3GPP Long Term Evolution standard for uplink transmission [2].

Rich multipath components, however, are required in the propagation environment for CPSC to achieve a significant gain in terms of BER. Unfortunately, this requirement may not be satisfied in general. Cyclic delay diversity (CDD) [7] is a simple yet effective technique to solve this problem. By transmitting the same signal from multiple antennas equipped in a single transmitter with different cyclic delays, a multiple-input channel is equivalently transformed to a single-input one with increasing multipath diversity and without altering the receiver structure. For CDD-CPSC, the zero-forcing (ZF) receiver fails to obtain any diversity gain, while the ML and

MMSE receivers are able to pick up diversity gains under some conditions, as pure CPSC without CDD. To maximize the performance gain of applying CDD to CPSC systems, non-linear equalizers, such as the frequency-domain Turbo equalizer [8] and the block iterative generalized decision feedback equalizer [9], were developed. In cooperative CPSC systems, distributed CDD can be implemented via multiple single-antenna transmitters [10]. The idea of distributed CDD was further applied to physical-layer security enhancement [11] and spectrum sharing systems [12]. It is worth noting that all of the above-mentioned CDD transmission schemes are based on multiple local or distributed transmit antennas, each equipped with a radio frequency (RF) chain. This configuration obviously complicates the system implementation, expands the hardware cost, and increases the power consumption, which may be unfavorable for energy-constrained and size-limited devices.

Recently, reconfigurable intelligent surface (RIS)-assisted transmission has emerged as an easy-to-implement, low-cost, and green communication technique [13], [14], [15]. On an RIS, there are a large number of passive reflecting elements, each of which is able to reflect and exert adjustable amplitude-phase changes on incident signals. In this sense, the amplitude-phase responses of RISs and associated channels can be reconfigured intentionally to achieve different purposes [16]. By exploiting this property, RISs have been applied to enhance the wireless communications in terms of energy efficiency [17], [18], weighted sum-rate [19], secrecy rate [20], [21], [22], network coverage [23], error performance [24], localization accuracy [25], etc. In particular, an RIS can be considered as an RF chain-free multi-antenna device. Inspired by this observation, the authors in [26] and [27] designed RIS-based multiple-input multiple-output transmission schemes for spatial multiplexing and Alamouti space–time block coding, respectively. On the other hand, the idea of index modulation (IM) [28], which uses the indices of some resources/building blocks (e.g., antennas, subcarriers, time slots, and signal constellations) to convey information, has been introduced into RIS-aided communications. Obviously, RISs can be explicitly deployed to enhance the existing IM schemes [29], [30], [31]. Moreover, new RIS-based IM schemes that use the indices of reflection patterns to carry information were developed in [32], [33], [34], [35], [36], [37], [38], [39], and [40]. In contrast to the above-mentioned RIS-related works that focus on narrowband wireless communications over flat fading channels, the authors in [41], [42], and [43] studied RIS-aided OFDM broadband wireless communications, in which the channel state information (CSI) is estimated in the frequency domain without multipath diversity gains.

To the best of our knowledge, CPSC transmission techniques have not been investigated for RIS-aided broadband wireless communications. Moreover, there have not been any reports of time-domain channel estimation methods for RIS-aided broadband frequency-selective channels in the literature. The fact that an RIS acts as a multi-element reflector has also not been exploited to implement CDD as well. Since OFDM and CPSC have different pros and cons, CPSC-RIS can be considered as an alternative to OFDM-RIS. They can coexist and complement each other for broadband communications. Against this background, we design a CPSC transmission scheme for RIS-empowered broadband wireless systems in this paper. However, the CP occupies a non-negligible bandwidth and leads to a reduction of the spectral efficiency (SE), which is a notable problem especially for short-packet communications. To solve this problem, we further develop an extension of CPSC-RIS by resorting to the concept of IM. Specifically, the main contributions of this paper are summarized as follows:

- A CPSC transmission scheme with CDD and phase shift keying (PSK) signaling is proposed for RIS-empowered broadband wireless systems to harvest multipath diversity gains. An efficient pilot-aided channel estimator, which is able to estimate the equivalent channel in the time domain via one transmission block, is developed for CPSC-RIS. In this sense, CPSC-RIS provides a new framework of channel estimation for RIS-aided broadband communications systems.
- The proposed CPSC-RIS scheme provide a flexible design. By adjusting the block size, CPSC-RIS can adapt to different degrees of variability in the CSI. In particular, CPSC-RIS with a small block size can be dedicated to short-packet communications at the cost of some diversity gains. On the other hand, compared with conventional antenna-based CDD-CPSC, CPSC-RIS uses the RIS to achieve CDD, avoiding multiple complicated and power-hungry RF chains.
- Both ML and ZF/MMSE detectors are designed for CPSC-RIS. We analyze the BER performance of CPSC-RIS over frequency-selective Nakagami-m fading channels. An upper bound on the BER of CPSC-RIS is derived in closed-form by assuming the ML detection without channel estimation errors. From the BER analysis, the diversity order and the performance improvement of CPSC-RIS over CPSC is characterized.
- An extension of CPSC-RIS, termed CPSC-RIS-IM, is also proposed to improve the SE by resorting to the concept of IM. To be more specific, CPSC-RIS-IM encodes the cyclic delays caused by the RIS for conveying additional information. A low-complexity detector is then designed for CPSC-RIS-IM.

The remainder of this paper is organized as follows. Section II describes the system model of CPSC-RIS, including the designs of channel estimator and signal detectors. The performance of CPSC-RIS with the ML detection is analyzed in Section III, followed by one IM-empowered extension of CPSC-RIS in Section IV. Section V presents the computer simulation results, and finally, Section VI concludes the paper.

Notations: Column vectors and matrices are denoted by lowercase and uppercase boldface letters, respectively. Superscripts $(\cdot)^*$, $(\cdot)^T$, and $(\cdot)^H$ stand for conjugate, transpose, and Hermitian transpose, respectively. The $N \times N$ identity matrix is symbolized by $\mathbf{I}_{N\times N}$. $\mathbf{1}_{1\times N}$ and $\mathbf{0}_{1\times N}$ denote an all-one matrix and an all-zero matrix of size $1 \times N$, respectively. $\mathrm{diag}\{\cdot\}$ transforms a vector into a diagonal matrix. $\Re\{\cdot\}$ and $\Im\{\cdot\}$ return the real and imaginary parts of a complex number, respectively. $j = \sqrt{-1}$ is the imaginary unit. $(\mathcal{C})\mathcal{N}(\mu, \sigma^2)$ represents the (complex) Gaussian distribution with mean μ and variance σ^2. The probability of an event and the probability density function (PDF) of a random variable are denoted by $\Pr(\cdot)$ and $p(\cdot)$, respectively. $E\{\cdot\}$ and $Var\{\cdot\}$ denote expectation and variance, respectively. $\|\cdot\|$ stands for the Frobenius norm. $Q(\cdot)$, $\Gamma(\cdot)$, and $\lfloor\cdot\rfloor$ represent the Gaussian

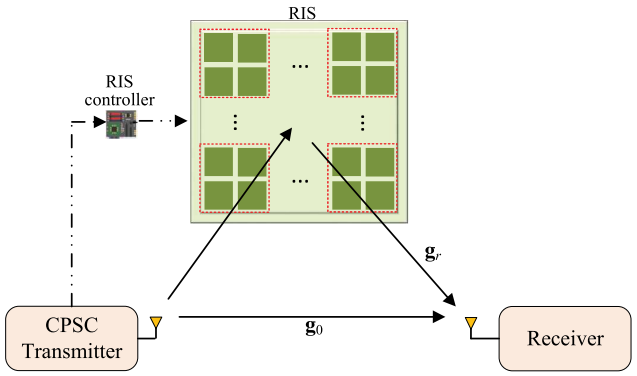

Fig. 1. The block diagram of the proposed CPSC-RIS system comprising a single-antenna transmitter, a multi-element RIS, and a single-antenna receiver.

Q-function, Gamma function, and floor function, respectively. $\mathrm{rank}(\cdot)$ and $\mathrm{Tr}(\cdot)$ denote the rank and trace of a matrix, respectively. $\odot$ represents the Hadamard product. $\angle(\cdot)$ denotes the phase of a complex number and $\mathrm{cir}(\cdot)$ denotes right circulant operation.

II. System Model

The block diagram of the proposed CPSC-RIS system is illustrated in Fig. 1, where a CPSC transmitter communicates with a receiver over frequency-selective block fading channels with the aid of an RIS. Both the transmitter and the receiver are equipped with a single antenna, while the RIS that is connected to a controller consists of N_R reflecting elements. The RIS controller follows the instructions from the transmitter to adjust the reflection coefficients of the RIS [16]. However, N_R is typically a large number, which results in high overhead/complexity for channel estimation and coefficient adjustment. Hence, we adopt the grouping method [41], [44], i.e., the total of N_R reflecting elements are partitioned into R reflecting groups, each of which consists of $N_G = N_R/R$ adjacent elements sharing a common reflection coefficient.[1] Accordingly, the reflection coefficient for the r-th group of the RIS is expressed as $\phi_r = a_r \exp(j\theta_r)$, where a_r is the amplitude coefficient and θ_r is the phase shift with $r = 1, \ldots, R$. For all r, we set a_r to unity and take $\theta_r \in [0, 2\pi)$ from a discrete set Θ.

The direct channel link from the transmitter to the receiver is described by the channel impulse response $\mathbf{g}_0 = [g_0(1), \ldots, g_0(L_0)]^T$, where L_0 is the number of channel taps for $\mathbf{g}_0$. The combined channel from the transmitter to the r-th reflecting group is assumed to be flat fading, and the equivalent channel of the cascaded transmitter-RIS-receiver link associated with the r-th reflecting group is given by $\mathbf{g}_r = [g_r(1), \ldots, g_r(L_r)]^T$ with L_r channel taps. In this paper, the amplitude of $g_{\bar{r}}(l_{\bar{r}})$ is modeled as a Nakagami-m distribution with fading parameter $m_{\bar{r}}(l_{\bar{r}}) \in [1, 2, \ldots, \infty]$ and spreading parameter $\Omega_{\bar{r}}(l_{\bar{r}}) > 0$, i.e.,

$$p_{|g_{\bar{r}}(l_{\bar{r}})|}(x) = \frac{2m_{\bar{r}}(l_{\bar{r}})^{m_{\bar{r}}(l_{\bar{r}})} x^{2m_{\bar{r}}(l_{\bar{r}})-1}}{\Omega_{\bar{r}}(l_{\bar{r}})^{m_{\bar{r}}(l_{\bar{r}})}\Gamma(m_{\bar{r}}(l_{\bar{r}}))} \exp\left(-\frac{m_{\bar{r}}(l_{\bar{r}})x^2}{\Omega_{\bar{r}}(l_{\bar{r}})}\right), \tag{1}$$

where $x > 0$, $\bar{r} = 0, 1, \ldots, R$, and $l_{\bar{r}} = 1, \ldots, L_{\bar{r}}$. Note that the phase of $g_{\bar{r}}(l_{\bar{r}})$ is not uniformly distributed [45], [46]; its PDF is given in [46] and assumed to be the same for all $\bar{r}$ and $l_{\bar{r}}$. Here, the channels associated with different reflecting groups are approximately considered as independent and identically distributed fading. We note that the practical case of correlated Nakagami-m fading [47] will be considered in future work.

A. Transmitter Design

For each transmission, the CPSC transmitter modulates $b = N\log_2(M)$ information bits into a symbol vector $\mathbf{x} = [x(1), \ldots, x(N)]^T$, where $x(n)$ is a normalized M-ary PSK symbol drawn from the constellation $\mathcal{X}$ for $n = 1, \ldots, N$. After adding an L-length CP to the beginning of $\mathbf{x}$, the transmitted data vector can be given by

$$\mathbf{x}_{CP} = [x(N-L+1), \ldots, x(N), x(1), \ldots, x(N)]^T, \tag{2}$$

where $L \geq \max\{L_0, \ldots, L_R\}$.[2] At this point, the transmitter derives the values of θ_r for all r based on $\mathbf{x}_{CP}$ and convey them to the RIS controller that further adjusts the R reflecting groups. It is worth noting that since $\mathbf{x}_{CP}$ is a PSK-modulated vector, cyclically delayed versions of $\mathbf{x}_{CP}$ can be constructed by performing phase shifts on $\mathbf{x}_{CP}$. To achieve CDD, θ_r is required to vary along with the transmission of $\mathbf{x}_{CP}$ and thus denoted by the vector $\boldsymbol{\theta}_r$ in the following. Moreover, by applying $\boldsymbol{\theta}_r$, the signal reflected from the r-th group of the RIS is expected to be a cyclically delayed version of $\mathbf{x}$, appended with an additional L-length CP, i.e.,

$$\mathbf{x}_{CP}(\Delta_r) = \Big[\underbrace{x(N-\Delta_r-L+1), \ldots, x(N-\Delta_r)}_{\text{CP}}, \underbrace{x(N-\Delta_r+1), \ldots, x(N), x(1), \ldots, x(N-\Delta_r)}_{\mathbf{x}(\Delta_r)}\Big]^T, \tag{3}$$

where $\mathbf{x}(\Delta_r)$ is the cyclically delayed version of $\mathbf{x}$ with the cyclic delay Δ_r for the r-th reflecting group. In CPSC-RIS, we let $\Delta_r = r\Delta$, where $L \leq \Delta \leq \lfloor N/(R+1) \rfloor$. Here, the constraint $\Delta \geq L$ is required to avoid inter-symbol interference (ISI) caused by multipath channels, while the constraint $\Delta \leq \lfloor N/(R+1) \rfloor$ is required to avoid ISI caused by simultaneous CPSC transmissions from different reflecting groups considering the block length. From $\mathbf{x}_{CP} \odot \exp(j\boldsymbol{\theta}_r) = \mathbf{x}_{CP}(\Delta_r)$, we have

$$\boldsymbol{\theta}_r = \Big[\angle x(N-\Delta_r-L+1) - \angle x(N-L+1), \ldots, \angle x(N-\Delta_r) - \angle x(N), \angle x(N-\Delta_r+1) - \angle x(1), \ldots, \angle x(N-\Delta_r) - \angle x(N)\Big]^T, \quad r = 1, \ldots, R \tag{4}$$

[1] In practice, the grouping should be implemented according to the statistical characteristics of channels. The value of N_G can be obtained by trial and error for achieving a good trade-off between complexity, SE, and error performance. Also, the number of reflecting elements in each group is not necessary to be equal. Although the grouping that merges N_G independent channels into a combined channel results in a loss of some diversity gains, the numbers of reflection coefficients and channel links that are required to be adjusted and estimated respectively are reduced from N_R to R, which significantly lowers the complexity of RIS configuration and channel estimation.

[2] The values of $L_0, \ldots, L_R$ are assumed to be known by using channel sounding schemes [10].

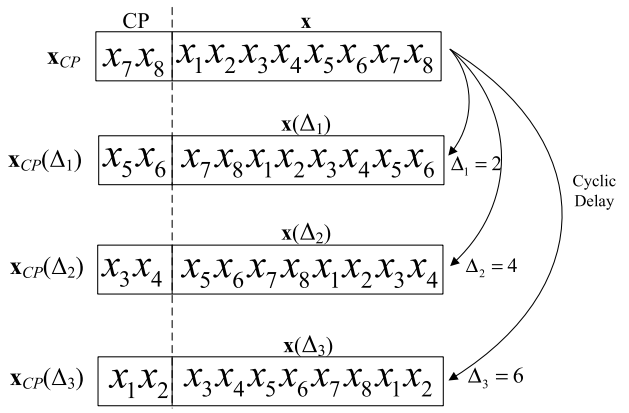

Fig. 2. An example of $\mathbf{x}_{CP}$ and $\mathbf{x}_{CP}(\Delta_r), r = 1, \ldots, R$ for CPSC-RIS, where $N = 8, R = 3$, and $\Delta = 2$. To save space, $x(n)$ is denoted by x_n in the figure and later in Fig. 4.

and

$$\Theta = \left\{0, \frac{2\pi}{M}, \cdots, \frac{2\pi(M-1)}{M}\right\}. \quad (5)$$

In Fig. 2, we present an illustrative example of $\mathbf{x}_{CP}$ and $\mathbf{x}_{CP}(\Delta_r), r = 1, \ldots, R$, where $N = 8, R = 3, \Delta = 2$, and $\mathbf{x}_{CP}(\Delta_r), r = 1, 2, 3$ are derived from $\mathbf{x}_{CP}$ via phase shifts.

At the receiver, after discarding the CP, the channel output is given by

$$\mathbf{y} = \mathbf{G}_0\mathbf{x} + \sum_{r=1}^{R} \mathbf{G}_r\mathbf{x}(\Delta_r) + \mathbf{w} = \sum_{\bar{r}=0}^{R} \mathbf{G}_{\bar{r}}\mathbf{x}(\Delta_{\bar{r}}) + \mathbf{w}, \quad (6)$$

where $\Delta_0 = 0$, $\mathbf{w} \in \mathbb{C}^{N\times 1}$ is the noise vector with the distribution $\mathcal{CN}(\mathbf{0}, N_0\mathbf{I}_{N\times N})$, and $\mathbf{G}_{\bar{r}}$ is an $N \times N$ circulant channel matrix given by $\mathbf{G}_{\bar{r}} = \mathrm{cir}(\mathbf{g}_{\bar{r}}^0)$ with $\mathbf{g}_{\bar{r}}^0 = [\mathbf{g}_{\bar{r}}^T, \mathbf{0}_{1\times(N-L_{\bar{r}})}]^T \in \mathbb{C}^{N\times 1}$. The signal-to-noise ratio (SNR) in this paper is defined as E_b/N_0 with $E_b = (N+L)/b$ being the average transmitted energy per bit. We can rewrite (6) as

$$\mathbf{y} = \sum_{\bar{r}=0}^{R} \mathbf{X}\mathbf{g}_{\bar{r}}^0(\Delta_{\bar{r}}) + \mathbf{w} = \mathbf{X}\mathbf{g}_{eq} + \mathbf{w}, \quad (7)$$

where $\mathbf{g}_{\bar{r}}^0(\Delta_{\bar{r}})$ is the cyclicly delayed version of $\mathbf{g}_{\bar{r}}^0$ with the cyclic delay $\Delta_{\bar{r}}$, $\mathbf{X}$ is an $N \times N$ circulant matrix represented by $\mathbf{X} = \mathrm{cir}(\mathbf{x})$, and $\mathbf{g}_{eq}$ is given by

$$\mathbf{g}_{eq} = \sum_{\bar{r}=0}^{R} \mathbf{g}_{\bar{r}}^0(\Delta_{\bar{r}}) = [\mathbf{g}_0^T, \mathbf{0}_{1\times(\Delta-L_0)}, \mathbf{g}_1^T, \mathbf{0}_{1\times(\Delta-L_1)}, \cdots, \mathbf{g}_R^T, \mathbf{0}_{1\times(N-R\Delta-L_R)}]^T. \quad (8)$$

From (8), provided that the cyclic delay constraints are satisfied, increasing the value of R enhances the channel impulse response (CIR). We also define $\mathbf{g}'_{eq} = [g'_{eq}(1), \ldots, g'_{eq}(L_s)]^T = [\mathbf{g}_0^T, \mathbf{g}_1^T, \ldots, \mathbf{g}_R^T]^T$, which consists of $L_s = \sum_{\bar{r}=0}^{R} L_{\bar{r}}$ non-zero entries of $\mathbf{g}_{eq}$. As seen from (6) and (7), the cyclic delays on $\mathbf{x}$ are converted into those on channels. By denoting $\mathbf{G}_{eq} = \mathrm{cir}(\mathbf{g}_{eq})$, (7) can be further expressed as

$$\mathbf{y} = \mathbf{G}_{eq}\mathbf{x} + \mathbf{w}. \quad (9)$$

It can be observed from (9) that CPSC-RIS can be regarded as a conventional CPSC scheme with the enhanced CIR in (8). Employing CDD does not change the characteristics of the transmitted signal. Obviously, the SE of CPSC-RIS is given by

$$\mathsf{F}_{\text{CPSC-RIS}} = \frac{b}{N+L} = \frac{N\log_2(M)}{N+L} \quad \text{bps/Hz}. \quad (10)$$

B. Receiver Design

In this subsection, we successively design a pilot-aided channel estimator and various detectors for CPSC-RIS.

1) Channel Estimator: For channel estimation, a pilot vector $\mathbf{x}_p \in \mathbb{C}^{N\times 1}$, instead of a data vector $\mathbf{x}$, is transmitted from the CPSC transmitter, and the RIS is configured similarly to (4). Based on (7), the least-square estimation of $\mathbf{g}_{eq}$ is given by

$$\hat{\mathbf{g}}_{eq} = \mathbf{X}_p^{-1}\mathbf{y} = \mathbf{g}_{eq} + \mathbf{g}_e, \quad (11)$$

where $\mathbf{X}_p = \mathrm{cir}(\mathbf{x}_p)$ and $\mathbf{g}_e = \mathbf{X}_p^{-1}\mathbf{w}$ represents the vector of channel estimation errors. $\mathbf{g}_e$ is independent of $\mathbf{g}_{eq}$ and follows the Gaussian distribution $\mathcal{CN}(\mathbf{0}, \sigma_e^2\mathbf{I}_{N\times N})$. The MSE of channel estimation can be derived as

$$\begin{aligned}\epsilon &= E\{\|\mathbf{g}_e\|^2\} \\ &= \mathrm{Tr}\left\{\mathbf{X}_p^{-1}E\{\mathbf{w}\mathbf{w}^H\}\left(\mathbf{X}_p^{-1}\right)^H\right\} \\ &= N_0\mathrm{Tr}\left\{\left(\mathbf{X}_p^H\mathbf{X}_p\right)^{-1}\right\}. \end{aligned} \quad (12)$$

Proposition 1: To minimize the MSE, $\mathbf{X}_p$ should satisfy $\mathbf{X}_p^H\mathbf{X}_p = N\mathbf{I}_{N\times N}$.

Proof: See Appendix A. ∎

In particular, using Zadoff-Chu sequences [48] as $\mathbf{x}_p$ meets the requirement. For N being an even number, we take $\mathbf{x}_p = [1, \exp(j\varpi\pi/N), \exp(j4\varpi\pi/N), \ \ldots, \ \exp(j\varpi\pi(N-1)^2/N)]^T$, where ϖ is an arbitrary integer relatively prime to N. Obviously, in this case, the achieved MSE is given by $\epsilon = N_0$ and we have $\sigma_e^2 = N_0/N$. In Fig. 3, we verify the theoretical analysis of MSE by comparing it with simulation results, where $N = 16, R = 4, m_{\bar{r}}(l_{\bar{r}}) = 3$, and $L_{\bar{r}} = 2$ for all $\bar{r}$ and $l_{\bar{r}}$ with an exponential-decay power-delay profile (PDP). It can be observed that the theoretical curve perfectly agrees with the simulation results for our proposed channel estimator.

As described above, the channel estimation for CPSC-RIS can be completed via a single block of pilots regardless of the value of R. This is much faster than existing frequency-domain channel estimation methods for RIS-aided broadband communications systems, such as the one in [42] that requires $R+1$ transmission blocks to extract the CSI. Moreover, such channel estimation framework applies to RIS-aided narrow-band communications, and achieves the same estimation accuracy with the same number of training symbols as the existing discrete Fourier transform (DFT)-based channel estimation scheme in [49]. In this sense, CPSC-RIS provides a novel framework of channel estimation for RIS-aided broadband and narrow-band communications. With CSI, various detectors can be developed to recover x, which will be described in the following.

2) ML Detector: From (7), the ML detector with the estimated CSI can be formulated as

$$\hat{\mathbf{x}} = \arg\min_{\mathbf{x}} \|\mathbf{y} - \mathrm{cir}(\mathbf{x})\hat{\mathbf{g}}_{eq}\|^2, \quad (13)$$

where $\hat{\mathbf{x}} = [\hat{x}(1), \ldots, \hat{x}(N)]^T$ is the estimate of $\mathbf{x}$. Since the ML detector makes a joint decision on the N M-ary PSK

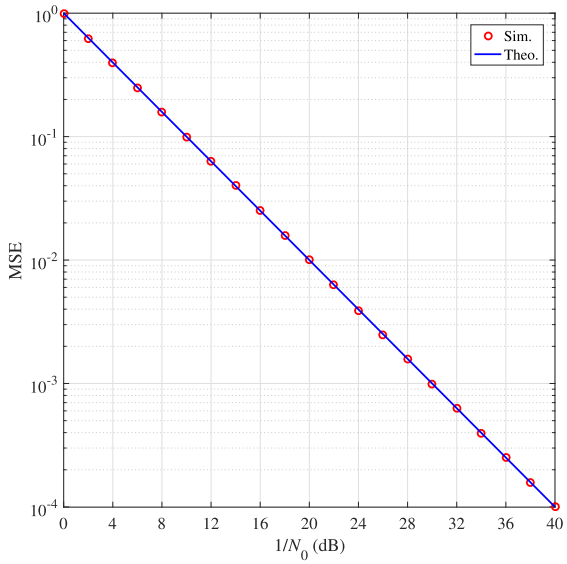

Fig. 3. MSE versus $1/N_0$ for CPSC-RIS, where $N = 16, R = 4$, $m_{\bar{r}}(l_{\bar{r}}) = 3$, and $L_{\bar{r}} = 2$ for all $\bar{r}$ and $l_{\bar{r}}$ with an exponentially decaying PDP.

symbols, the computational complexity in terms of complex multiplications is of order $\sim \mathcal{O}(M^N)$, which poses intolerable computational burden to the receiver. Thus, a low-complexity detector is highly recommended.

3) ZF/MMSE Detectors: Since $\mathbf{G}_{eq}$ is a circulant matrix, it has eigen decomposition $\mathbf{G}_{eq} = \mathbf{F}^H \mathbf{\Lambda} \mathbf{F}$, where $\mathbf{F}$ is the unitary DFT matrix with $\mathbf{F}^H\mathbf{F} = \mathbf{I}_{N\times N}$, and $\mathbf{\Lambda}$ is the diagonal matrix whose diagonal elements are the N-point (non-unitary) DFT of $\mathbf{g}_{eq}$, i.e.,

$$\lambda(k) = \sum_{n=1}^{N} g_{eq}(n) \exp\left(-j\frac{2\pi(n-1)(k-1)}{N}\right), \quad (14)$$

where $k = 1, \ldots, N$. Therefore, based on (9), the frequency-domain received signal can be written as

$$\mathbf{y}_F = [y_F(1), \ldots, y_F(N)]^T = \mathbf{F}\mathbf{y} = \mathbf{\Lambda}\mathbf{x}_F + \mathbf{w}_F, \quad (15)$$

where $\mathbf{x}_F$ and $\mathbf{w}_F$ are the frequency-domain counterparts of $\mathbf{x}$ and $\mathbf{w}$, respectively. For frequency-domain ZF/MMSE equalization, $\mathbf{y}_F$ is fed into N single-tap equalizers in parallel, each of which is simply realized by one complex-valued multiplication, i.e.,

$$\hat{x}_F(n) = \phi(n) y_F(n), \quad n = 1, \ldots, N \quad (16)$$

where $\hat{x}_F(n)$ is the output of the n-th equalizer, and $\phi(n) = \lambda(n)^*/(|\lambda(n)|^2 + cN_0)$ with $c = 1$ for MMSE equalizer and $c = 0$ for ZF equalizer. Finally, we arrive at the estimated time-domain symbol vector via

$$\hat{\mathbf{x}} = \mathbf{F}^H \hat{\mathbf{x}}_F, \quad (17)$$

where $\hat{\mathbf{x}}_F = [\hat{x}_F(1), \ldots, \hat{x}_F(N)]^T$.

Obviously, by using single-tap equalization and existing efficient algorithms with the implementation of the DFT, the ZF/MMSE detectors achieve much lower computational complexity than the ML detector in (13). As a compromise, the ZF/MMSE detectors perform worse than the ML detector in terms of BER performance. Since CPSC-RIS can be regarded as a conventional CPSC scheme with enhanced CIR, the behaviors of ZF, ML, and MMSE detectors for CPSC-RIS are similar to those for conventional CPSC schemes. Particularly, the ML and MMSE detectors are able to harvest some diversity gains, while the ZF detector cannot extract any multipath diversity since the equalization severely amplifies the noise at frequencies in deep fades [4].

III. Performance Analysis

In this section, we concentrate on the performance analysis of the ML detector for CPSC-RIS. An upper bound on the BER of CPSC-RIS in the absence of channel estimation errors is provided after deriving the pairwise error probability (PEP) in closed-form.

Let us first study the conditional PEP with channel estimation errors, namely $\Pr(\mathbf{X} \to \hat{\mathbf{X}}|\hat{\mathbf{g}}_{eq})$, which is the probability of detecting $\mathbf{X}$ as $\hat{\mathbf{X}}$ conditioned on $\hat{\mathbf{g}}_{eq}$. From (7), (9), and (13), we have

$$\Pr\left(\mathbf{X} \to \hat{\mathbf{X}}|\hat{\mathbf{g}}_{eq}\right) = \Pr\left(\|\mathbf{y} - \mathbf{X}\hat{\mathbf{g}}_{eq}\|^2 > \left\|\mathbf{y} - \hat{\mathbf{X}}\hat{\mathbf{g}}_{eq}\right\|^2\right). \quad (18)$$

Based on (11), $\mathbf{y}$ can be expressed as

$$\mathbf{y} = \mathbf{X}(\hat{\mathbf{g}}_{eq} - \mathbf{g}_e) + \mathbf{w} = \mathbf{X}\hat{\mathbf{g}}_{eq} + \bar{\mathbf{w}}, \quad (19)$$

where $\bar{\mathbf{w}} = -\mathbf{X}\mathbf{g}_e + \mathbf{w}$. After putting (19) into (18), we are led to

$$\begin{aligned}\Pr\left(\mathbf{X} \to \hat{\mathbf{X}}|\hat{\mathbf{g}}_{eq}\right) &= \Pr\Bigg(-\left\|(\mathbf{X} - \hat{\mathbf{X}})\hat{\mathbf{g}}_{eq}\right\|^2 \\ &\qquad -2\Re\left\{\bar{\mathbf{w}}^H(\mathbf{X} - \hat{\mathbf{X}})\hat{\mathbf{g}}_{eq}\right\} > 0\Bigg) \\ &= \Pr(V > 0). \end{aligned} \quad (20)$$

We observe that V is Gaussian distributed with

$$E\{V\} = -\left\|(\mathbf{X} - \hat{\mathbf{X}})\hat{\mathbf{g}}_{eq}\right\|^2,$$

$$Var\{V\} = 2\,N_0\left\|(\mathbf{X} - \hat{\mathbf{X}})\hat{\mathbf{g}}_{eq}\right\|^2 + 2\sigma_e^2\left\|\mathbf{X}^H(\mathbf{X} - \hat{\mathbf{X}})\hat{\mathbf{g}}_{eq}\right\|^2.$$

Therefore, (20) can be calculated as

$$\Pr\left(\mathbf{X} \to \hat{\mathbf{X}}|\hat{\mathbf{g}}_{eq}\right) = Q\left(\frac{\left\|(\mathbf{X} - \hat{\mathbf{X}})\hat{\mathbf{g}}_{eq}\right\|^2}{\sqrt{2N_0\left\|(\mathbf{X} - \hat{\mathbf{X}})\hat{\mathbf{g}}_{eq}\right\|^2 + 2\sigma_e^2\left\|\mathbf{X}^H(\mathbf{X} - \hat{\mathbf{X}})\hat{\mathbf{g}}_{eq}\right\|^2}}\right). \quad (21)$$

In order to obtain the unconditional PEP, (21) should be further averaged over $\hat{\mathbf{g}}_{eq}$. However, it is very difficult to derive a closed-form expression. Here, we consider the case of perfect channel estimation, i.e., $\sigma_e^2 = 0$.

In the absence of channel estimation errors, (21) reduces to

$$\Pr\left(\mathbf{X} \to \hat{\mathbf{X}}|\mathbf{g}_{eq}\right) = Q\left(\sqrt{\frac{\left\|(\mathbf{X} - \hat{\mathbf{X}})\mathbf{g}_{eq}\right\|^2}{2N_0}}\right). \quad (22)$$

The squared norm $\|(\mathbf{X}-\hat{\mathbf{X}})\mathbf{g}_{eq}\|^2$ can equivalently be developed as

$$\begin{aligned}\left\|\left(\mathbf{X}-\hat{\mathbf{X}}\right)_{[L_s]}\mathbf{g}'_{eq}\right\|^2 &= \mathbf{g}'^H_{eq}\mathbf{A}\mathbf{g}'_{eq}\\ &= \mathbf{g}'^H_{eq}\mathbf{U}^H\mathbf{D}\mathbf{U}\mathbf{g}'_{eq}\\ &= \sum_{l=1}^{L_s} d(l)|\tilde{g}_{eq}(l)|^2, \end{aligned} \tag{23}$$

where $(\mathbf{X}-\hat{\mathbf{X}})_{[L_s]}$ comprises L_s columns of $(\mathbf{X}-\hat{\mathbf{X}})$ corresponding to L_s non-zero entries of $\mathbf{g}_{eq}$, $\mathbf{A}=(\mathbf{X}-\hat{\mathbf{X}})^H_{[L_s]}(\mathbf{X}-\hat{\mathbf{X}})_{[L_s]}$ is decomposed as $\mathbf{A}=\mathbf{U}^H\mathbf{D}\mathbf{U}$ with $\mathbf{U}$ being a unitary matrix and $\mathbf{D}=\mathrm{diag}\{d(1),\ldots,d(L_s)\}$, and $\tilde{\mathbf{g}}_{eq}=[\tilde{g}_{eq}(1),\ldots,\tilde{g}_{eq}(L_s)]^T=\mathbf{U}\mathbf{g}'_{eq}$. Hence, (22) can be rewritten as

$$\Pr\left(\mathbf{X}\to\hat{\mathbf{X}}|\mathbf{g}_{eq}\right)=Q\left(\sqrt{\frac{\sum_{l=1}^{L_s}d(l)|\tilde{g}_{eq}(l)|^2}{2N_0}}\right), \tag{24}$$

where $\tilde{g}_{eq}(l)=\mathbf{u}_l^T\mathbf{g}'_{eq}$ with $\mathbf{u}_l=[u_{l1},\ldots,u_{lL_s}]^T$ and $u_{ll'}$ being the (l,l')-th element of $\mathbf{U}$ for $l,l'=1,\ldots,L_s$. Next, the approximations in [46] are used to derive the moment generating function (MGF) of $|\tilde{g}_{eq}(l)|^2$. Specifically, the real and imaginary parts of a complex Nakagami-m fading gain can be approximated as $\mathcal{N}(\mu_X,\Omega_s/2)$ and $\mathcal{N}(\mu_Y,\Omega_s/2)$ distributions, respectively, where $\mu_X=\sqrt{\sqrt{1-1/m}\Omega}\cos\phi$, $\mu_Y=\sqrt{\sqrt{1-1/m}\Omega}\sin\phi$, and $\Omega_s=\Omega(1-\sqrt{1-1/m})$ with m being the fading parameter, Ω being the spreading parameter, and ϕ being the angle parameter of the complex Nakagami-m distribution. Hence, by defining $\mu_X(l)$, $\mu_Y(l)$, and $\Omega_s(l)$ as the corresponding parameters that are associated with $g'_{eq}(l)$, we have $\Re\{\tilde{g}_{eq}(l)\}\sim\mathcal{N}(\Re\{\mathbf{u}_l^T\boldsymbol{\mu}\},\mathbf{u}_{2l}^T\boldsymbol{\Omega}_s/2)$ and $\Im\{\tilde{g}_{eq}(l)\}\sim\mathcal{N}(\Im\{\mathbf{u}_l^T\boldsymbol{\mu}\},\mathbf{u}_{2l}^T\boldsymbol{\Omega}_s/2)$, where $\boldsymbol{\mu}=[\mu_X(1)+j\mu_Y(1),\ldots,\mu_X(L_s)+j\mu_Y(L_s)]^T$, $\mathbf{u}_{2l}=[|u_{l1}|^2,\ldots,|u_{lL_s}|^2]^T$, and $\boldsymbol{\Omega}_s=[\Omega_s(1),\ldots,\Omega_s(L_s)]^T$. Hence, the MGF of $|\tilde{g}_{eq}(l)|^2$ can be given by

$$\mathcal{M}_l(t)=\frac{1}{1-t\mathbf{u}_{2l}^T\boldsymbol{\Omega}_s}\exp\left(\frac{t|\mathbf{u}_l^T\boldsymbol{\mu}|^2}{1-t\mathbf{u}_{2l}^T\boldsymbol{\Omega}_s}\right). \tag{25}$$

It can be shown that $|\mathbf{u}_l^T\boldsymbol{\mu}|^2$ in (25) is irrelevant to the value of ϕ. By using the well-known approximation $Q(x)\approx 1/12\cdot e^{-x^2/2}+1/4\cdot e^{-2x^2/3}$ [50], the unconditional PEP can be derived as

$$\begin{aligned}\Pr\left(\mathbf{X}\to\hat{\mathbf{X}}\right) &\approx E\left\{\tfrac{1}{12}\prod_{l=1}^{L_s}\exp\left(-\tfrac{d(l)|\tilde{g}_{eq}(l)|^2}{4N_0}\right)\right.\\ &\quad\left.+\tfrac{1}{4}\prod_{l=1}^{L_s}\exp\left(-\tfrac{d(l)|\tilde{g}_{eq}(l)|^2}{3N_0}\right)\right\}\\ &=\tfrac{1}{12}\prod_{l=1}^{L_s}\mathcal{M}_l\left(-\tfrac{d(l)}{4N_0}\right)+\tfrac{1}{4}\prod_{l=1}^{L_s}\mathcal{M}_l\left(-\tfrac{d(l)}{3N_0}\right), \end{aligned} \tag{26}$$

where $\tilde{g}_{eq}(l), l=1,\ldots,L_s$ are approximately regarded as independent from each other. Finally, according to the union bounding technique, the BER of CPSC-RIS can be upper bounded by

$$P_e\le\frac{1}{b2^b}\sum_{\mathbf{X}}\sum_{\hat{\mathbf{X}}}\Pr\left(\mathbf{X}\to\hat{\mathbf{X}}\right)\xi\left(\mathbf{X},\hat{\mathbf{X}}\right), \tag{27}$$

where $\xi(\mathbf{X},\hat{\mathbf{X}})$ is the number of erroneous bits when $\mathbf{X}$ is detected as $\hat{\mathbf{X}}$.

Remark 1: The contribution of L_s independent modified channel taps of $\tilde{\mathbf{g}}_{eq}$ to the unconditional PEP in (26) suggests that the highest possible diversity order is equal to L_s. However, this maximum diversity order is achieved if and only if $d(l)$ are non-null for all l, $\mathbf{X}$, and $\hat{\mathbf{X}}$. In general, the diversity order achieved by CPSC-RIS is given by $\min\mathrm{rank}(\mathbf{A})$. Since there exist a number of error events, such as

$$\mathbf{X}=\begin{bmatrix}1&1&\cdots&1\\1&1&\cdots&1\\\vdots&\vdots&\ldots&\vdots\\1&1&\cdots&1\\1&1&\cdots&1\end{bmatrix},\quad \hat{\mathbf{X}}=\begin{bmatrix}-1&-1&\cdots&-1\\-1&-1&\cdots&-1\\\vdots&\vdots&\ldots&\vdots\\-1&-1&\cdots&-1\\-1&-1&\cdots&-1\end{bmatrix},$$

which make $\mathrm{rank}(\mathbf{A})=1$, the asymptotic (i.e., at infinite SNR) diversity order of CPSC-RIS is equal to one. Since this type of error event rarely occurs, computer simulations in Section V will show that the multipath diversity can be extracted by CPSC-RIS for moderate BER values and reasonably large values of N.

On the other hand, compared with conventional CPSC systems without RIS and CDD, CPSC-RIS involves extra R RIS's reflecting links with $\sum_{\bar{r}=1}^{R}L_{\bar{r}}$ channel taps that are collected through CDD. Therefore, from (26) with $L_s\gg L_0$, the BER performance of CPSC-RIS is expected to be much better than that of conventional CPSC systems without RIS and CDD.

IV. IM-Empowered CPSC-RIS System

In this section, we extend CPSC-RIS to CPSC-RIS-IM, which improves the SE of CPSC-RIS by employing the concept of CDD-IM [51]. In CPSC-RIS-IM, the information bits are modulated into the cyclic delays at the RIS in addition to conventional constellation information of N PSK symbols. Specifically, a total of b information bits are divided into two parts. The first part, consisting of $b_1=\lfloor\log_2(R!)\rfloor$ bits, is used for permuting the cyclic delays at the RIS. Unlike the CPSC-RIS scheme in which the cyclic delay for the r-th reflecting group is fixed to $\Delta_r=r\Delta$, the cyclic delay for the r-th reflecting group in CPSC-RIS-IM is given by

$$\Delta_r=k_r\Delta, \tag{28}$$

where $r=1,\ldots,R$ and $\mathbf{k}=[k_1,k_2,\ldots,k_R]^T$ is a full permutation of $\{1,2,\ldots,R\}$ determined by the b_1 bits. The mapping from b_1 bits to $\mathbf{k}$ can be realized by either a look-up table or the permutation method [52]. Table I presents an example of a mapping table between the b_1 bits and $\mathbf{k}$ for $R=3$ and $b_1=2$, where the last two permutations are unused.

The second part, comprised of $b_2=N\log_2(M)$ bits, is mapped to N PSK symbols $\mathbf{x}=[x(1),\ldots,x(N)]^T$ via the regular M-PSK constellation $\mathcal{X}$ that is also used in CPSC-RIS. Therefore, the SE of CPSC-RIS-IM is given by

$$\mathsf{F}_{\text{CPSC-RIS-IM}}=\frac{N\log_2(M)+\lfloor\log_2(R!)\rfloor}{N+L}\ \text{bps/Hz}, \tag{29}$$

TABLE I
AN EXAMPLE OF MAPPING TABLE BETWEEN p_1 BITS AND $\mathbf{k}$ FOR $R = 3$

b_1 bits	$\mathbf{k}$
[0 0]	$[1,2,3]^T$
[0 1]	$[2,1,3]^T$
[1 0]	$[1,3,2]^T$
[1 1]	$[2,3,1]^T$
–	$[3,2,1]^T$
–	$[3,1,2]^T$

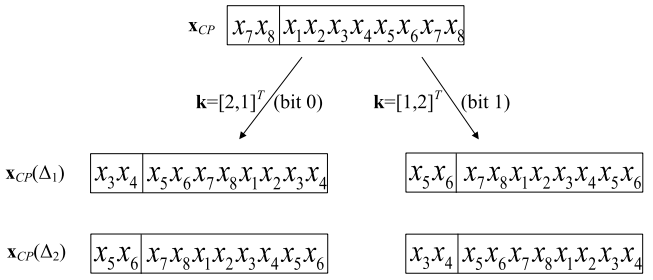

Fig. 4. Examples of $\mathbf{x}_{CP}$ and $\mathbf{x}_{CP}(\Delta_r), r = 1, \ldots, R$ for CPSC-RIS-IM with $\mathbf{k} = [2,1]^T$ and $\mathbf{k} = [1,2]^T$, where $N = 8, R = 2$, and $\Delta = 2$.

which shows that CPSC-RIS-IM can transmit $\lfloor \log_2(R!) \rfloor$ more bits per block transmission than CPSC-RIS. Obviously, increasing the value of R leads to higher SE. However, a larger value of R also incurs higher complexity of implementing the mapping between the b_1 bits and $\mathbf{k}$ at the transceiver, cyclic delays at the RIS, and signal detection at the receiver.

In Fig. 4, we present an example of $\mathbf{x}_{CP}$ and $\mathbf{x}_{CP}(\Delta_r), r = 1, \ldots, R$ for CPSC-RIS-IM, where $N = 8, R = 2, \Delta = 2$, and both two possible realizations of $\mathbf{k}$ are considered. It should be noted that there is ambiguity at the receiver to detect $\mathbf{x}$ and $\mathbf{k}$. We exemplify this point with Fig. 4 and letting $x(1) = x(2) = \cdots = x(8)$. Obviously, in this case, both $\mathbf{x}_{CP}(\Delta_1)$ and $\mathbf{x}_{CP}(\Delta_2)$ for $\mathbf{k} = [2,1]^T$ are completely the same as those for $\mathbf{k} = [1,2]^T$. Hence, we take the first symbol of $\mathbf{x}$, namely $x(1)$, as an anchor point to avoid ambiguity in signal detection. Specifically, instead of $\mathbf{x}$, we transmit $\tilde{\mathbf{x}} = \mathbf{x} \odot [\exp(j\pi/M), \mathbf{1}_{1\times(N-1)}]^T$ at the CPSC transmitter. In this manner, the Euclidean distance between $x(1)$ and any other symbols in $\tilde{\mathbf{x}}$ is maximized.

Similar to (7), the received signal for CPSC-RIS-IM can be expressed as

$$\mathbf{y} = \tilde{\mathbf{X}}\mathbf{g}_{eq,\mathbf{k}} + \mathbf{w}, \tag{30}$$

where the notations are defined in (7) except that $\tilde{\mathbf{X}} = \mathrm{cir}(\tilde{\mathbf{x}})$ and $\mathbf{g}_{eq,\mathbf{k}}$ is revised as

$$\mathbf{g}_{eq,\mathbf{k}} = \sum_{\bar{r}=0}^{R} \mathbf{g}_{\bar{r}}^0(k_r\Delta), \tag{31}$$

where $k_0 = 0$. Based on (30), ML and low-complexity detectors can be designed for CPSC-RIS-IM, which are discussed in the following.

A. ML Detector

The optimal ML detector makes a joint decision on $\mathbf{k}$ and $\mathbf{x}$ by searching all possible combinations of them, namely

$$\left(\hat{\mathbf{x}}, \hat{\mathbf{k}}\right) = \arg\min_{\mathbf{x},\mathbf{k}} \left\|\mathbf{y} - \tilde{\mathbf{X}}\mathbf{g}_{eq,\mathbf{k}}\right\|^2, \tag{32}$$

where $\hat{\mathbf{x}}$ and $\hat{\mathbf{k}}$ are the estimates of $\mathbf{x}$ and $\mathbf{k}$, respectively. Then, the corresponding b information bits can be readily recovered from $\hat{\mathbf{x}}$ and $\hat{\mathbf{k}}$. Obviously, the ML detector should search all $R!M^N$ possible combinations of $\mathbf{x}$ and $\mathbf{k}$ to find out the one that minimizes the ML metric, which results in the computational complexity in terms of complex multiplications of order $\sim \mathcal{O}(R!M^N)$ per block transmission. To lower the computational complexity, we next develop a low-complexity detector.

B. Low-Complexity Detector

For a realization of $\mathbf{k}$, denoted by $\mathbf{k}_i, i = 1, \ldots, 2^{b_1}$, we can employ the ZF/MMSE detectors similar to (15)-(17) for obtaining the estimate of $\tilde{\mathbf{x}}$, denoted by $\hat{\tilde{\mathbf{x}}}_{\mathbf{k}_i}$. Further, given $\mathbf{k}_i$, $\mathbf{x}$ is estimated as $\hat{\mathbf{x}}_{\mathbf{k}_i} = [\hat{x}_{\mathbf{k}_i}(1), \ldots, \hat{x}_{\mathbf{k}_i}(N)]^T = \hat{\tilde{\mathbf{x}}}_{\mathbf{k}_i} \odot [\exp(-j\pi/M), \mathbf{1}_{1\times(N-1)}]^T$. Then, each symbol in $\hat{\mathbf{x}}_{\mathbf{k}_i}$ is demodulated independently via M-PSK demodulation, namely

$$\hat{s}_{\mathbf{k}_i}(n) = \arg\min_{s\in\mathcal{X}} \|\hat{x}_{\mathbf{k}_i}(n) - s\|^2, \quad n = 1, \ldots, N \tag{33}$$

where $\hat{s}_{\mathbf{k}_i}(n)$ represents the hard decision on $\hat{x}_{\mathbf{k}_i}(n)$. Based on $\hat{\mathbf{s}}_{\mathbf{k}_i} = [\hat{s}_{\mathbf{k}_i}(1), \ldots, \hat{s}_{\mathbf{k}_i}(N)]^T$, the metric that $\mathbf{k}_i$ is used at the transmitter can be given by

$$T(\mathbf{k}_i) = \left\|\mathbf{y} - \hat{\tilde{\mathbf{S}}}_{\mathbf{k}_i}\mathbf{g}_{eq,\mathbf{k}_i}\right\|^2, \tag{34}$$

where $\hat{\tilde{\mathbf{S}}}_{\mathbf{k}_i} = \mathrm{cir}(\hat{\tilde{\mathbf{s}}}_{\mathbf{k}_i})$ with $\hat{\tilde{\mathbf{s}}}_{\mathbf{k}_i} = \hat{\mathbf{s}}_{\mathbf{k}_i} \odot [\exp(j\pi/M), \mathbf{1}_{1\times(N-1)}]^T$. Finally, the estimates of $\mathbf{k}$ and $\mathbf{x}$ can be expressed as

$$\hat{\mathbf{k}} = \min_{\mathbf{k}_i} T(\mathbf{k}_i), \tag{35}$$

and $\hat{\mathbf{x}} = \hat{\mathbf{s}}_{\hat{\mathbf{k}}}$, respectively.

C. Performance Analysis

Here, we analyze the BER performance of ML detection for CPSC-RIS-IM. Let us first define a permutation matrix $\mathbf{P}_{\mathbf{k}}$, which is made up of N columns of $\mathbf{I}_{N\times N}$ and satisfies $\mathbf{P}_{\mathbf{k}}\mathbf{g}_{eq} = \mathbf{g}_{eq,\mathbf{k}}$. Then, (30) can be rewritten as

$$\mathbf{y} = \tilde{\mathbf{X}}\mathbf{P}_{\mathbf{k}}\mathbf{g}_{eq} + \mathbf{w}. \tag{36}$$

In the case of perfect channel estimation, similar to (22), the conditional PEP can be written as

$$\begin{aligned}
&\Pr\left((\tilde{\mathbf{X}}, \mathbf{k}) \to (\hat{\tilde{\mathbf{X}}}, \hat{\mathbf{k}}) | \mathbf{g}_{eq}\right) \\
&\quad = \Pr\left(\left\|\mathbf{y} - \tilde{\mathbf{X}}\mathbf{P}_{\mathbf{k}}\mathbf{g}_{eq}\right\|^2 > \left\|\mathbf{y} - \hat{\tilde{\mathbf{X}}}\mathbf{P}_{\hat{\mathbf{k}}}\mathbf{g}_{eq}\right\|^2\right) \\
&\quad = Q\left(\sqrt{\frac{\left\|\left(\tilde{\mathbf{X}}\mathbf{P}_{\mathbf{k}} - \hat{\tilde{\mathbf{X}}}\mathbf{P}_{\hat{\mathbf{k}}}\right)\mathbf{g}_{eq}\right\|^2}{2N_0}}\right).
\end{aligned} \tag{37}$$

The unconditional PEP, namely $\Pr((\tilde{\mathbf{X}}, \mathbf{k}) \to (\hat{\tilde{\mathbf{X}}}, \hat{\mathbf{k}}))$, can be obtained by following the methods in (23)-(26), which is omitted to avoid redundancy. Finally, an upper bound on the BER of CPSC-RIS-IM is given by

$$P_e \le \frac{1}{b2^b} \sum_{\tilde{\mathbf{X}},\mathbf{k}} \sum_{\hat{\tilde{\mathbf{X}}},\hat{\mathbf{k}}} \Pr\left((\tilde{\mathbf{X}}, \mathbf{k}) \to (\hat{\tilde{\mathbf{X}}}, \hat{\mathbf{k}})\right) \xi\left((\tilde{\mathbf{X}}, \mathbf{k}), (\hat{\tilde{\mathbf{X}}}, \hat{\mathbf{k}})\right), \tag{38}$$

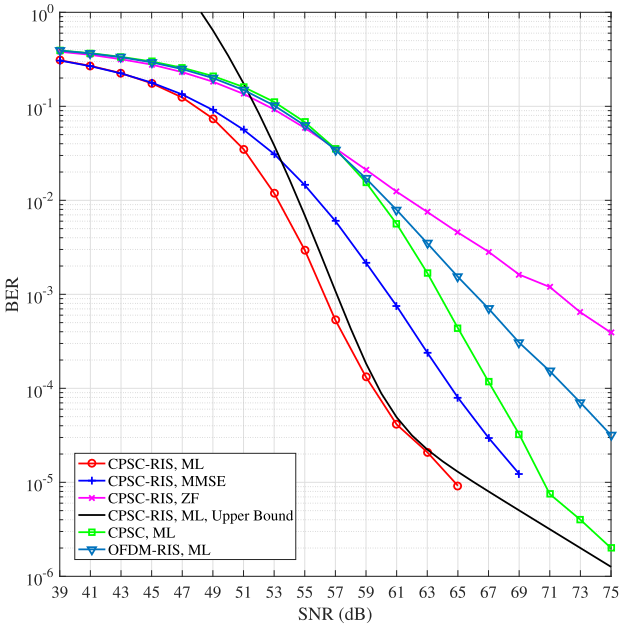

Fig. 5. Performance comparison among CPSC-RIS, CPSC, and OFDM-RIS with $N = 8, M = 2, R = 2$, and perfect CSI at the receiver.

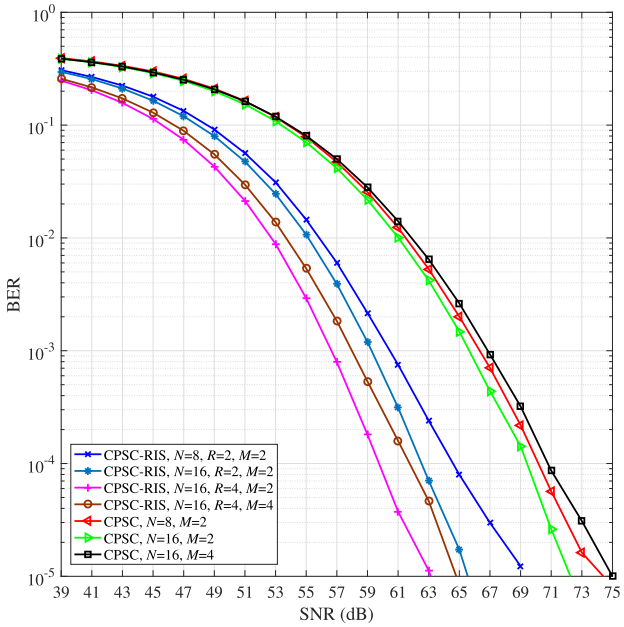

Fig. 6. Performance comparison between CPSC-RIS and CPSC with $N = 8, 16, M = 2, 4, R = 2, 4$, and perfect CSI at the receiver.

where $\xi((\tilde{\mathbf{X}}, \mathbf{k}), (\hat{\tilde{\mathbf{X}}}, \hat{\mathbf{k}}))$ is the number of erroneous bits when $(\tilde{\mathbf{X}}, \mathbf{k})$ is detected as $(\hat{\tilde{\mathbf{X}}}, \hat{\mathbf{k}})$.

Remark 2: In CPSC-RIS and CPSC-RIS-IM, the amplitude coefficients of all reflecting groups are fixed to 1, i.e., $a_r = 1$ for $r = 1, \ldots, R$. Actually, a reflection-type power amplifier can be deployed for each RIS element, such that a_r can be drawn from a discrete set, say $\{a^1, \ldots, a^t\}$ with all entries equal to or greater than 1 [53]. In this manner, the SE of CPSC-RIS and CPSC-RIS-IM can be further improved by encoding partial information (up to $R \log_2(t)$ bits) into the amplitude coefficients, and a multi-ring PSK constellation is observed at the receiver. Obviously, there is a trade-off between the SE and error performance.

V. Simulation Results

In this section, we conduct Monte Carlo simulations to evaluate the uncoded BER performance of CPSC-RIS(-IM) by taking CPSC and OFDM-RIS [42] as benchmarks. In OFDM-RIS, the RIS is configured to maximize the channel gain according to the method in [42] by assuming perfect CSI. In all simulations, we plot the BER versus SNR $= E_b/N_0$. We use $N_G = 8$, and increasing N_G is expected to improve the performance for a given value of R since the signal power reflected from each group is enhanced. The distances between the transmitter and the receiver, between the transmitter and the RIS, and between the RIS and the receiver are $D_0 = 54$ m, $D_1 = 5$ m, and $D_2 = 50$ m, respectively. The large-scale path loss of the transmitter-receiver, transmitter-RIS, and RIS-receiver links are given by $D_0^{-3.0}$, D_1^{-2}, and $D_2^{-2.7}$, respectively. All wireless channels are modeled by the exponentially decaying PDP with the decaying factor of unity, where each tap is generated according to the Nakagami-m distribution. For simplicity, we assume that $L_0 = \cdots = L_R = 2$, $m_0(1) = \cdots = m_0(L_0) = m_1(1) = \cdots = m_1(L_1) = \cdots = m_R(L_R) = 2$, and $\Delta = L$. Each BER point is obtained by averaging over at least 10^5 channel realizations.

Fig. 5 depicts the performance comparison among CPSC-RIS, CPSC, and OFDM-RIS, where $N = 8, M = 2$, $R = 2$, and perfect CSI is assumed at the receiver. CPSC-RIS employs the ML, MMSE, and ZF detectors, while CPSC and OFDM-RIS use the ML detectors. To verify the analysis given in Section III, we also plot the BER upper bound (27) as a theoretical bound for the ML detector of CPSC-RIS in Fig. 5. As seen from Fig. 5, for CPSC-RIS with the optimal ML detection, the BER upper bound agrees with the simulation results in the high SNR region. In particular, for CPSC-RIS, the ZF detector cannot harvest any diversity and performs the worst. In contrast, for CPSC-RIS, both the ML and MMSE detectors achieve diversity gains for practical BER values, while they fail to extract diversity gains at high SNR, i.e., the slopes of the BER curves change with increasing SNR. This is because the error events that result in a diversity order of unity are dominant only at high SNR. Moreover, CPSC-RIS even with low-complexity MMSE detector significantly outperforms conventional CPSC and OFDM-RIS with the optimal ML detectors throughout the considered SNR region. CPSC-RIS with the ML and MMSE detectors obtain approximately 8 dB and 3 dB SNR gains, respectively, over CPSC with the ML detector at a BER value of 10^{-4}. Since the MMSE detector is able to achieve acceptable performance with low implementation complexity, the MMSE-based detectors are adopted for CPSC-RIS(-IM) and CPSC in the remaining simulations.

Fig. 6 evaluates the BER performance of CPSC-RIS and CPSC, where $N = 8, 16, M = 2, 4, R = 2, 4$, and perfect CSI is assumed at the receiver. It can be observed from Fig. 6 that all considered CPSC-RIS schemes perform better than all CPSC schemes for all SNR values thanks to the extra R reflecting links introduced by the RIS, and the gain is more prominent for a larger value of R. For $N = 16$ and $M = 2$,

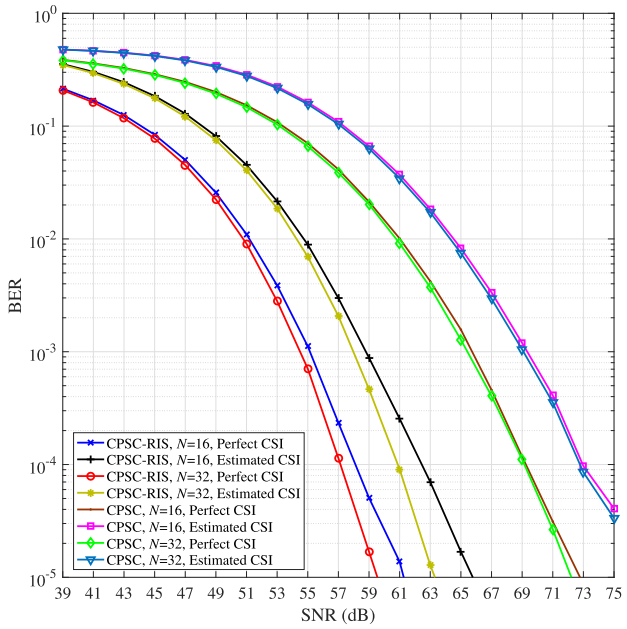

Fig. 7. Performance comparison between CPSC-RIS and CPSC with $N = 16, 32, M = 2$, and $R = 6$, where perfect channel estimation and practical channel estimation in (11) are considered.

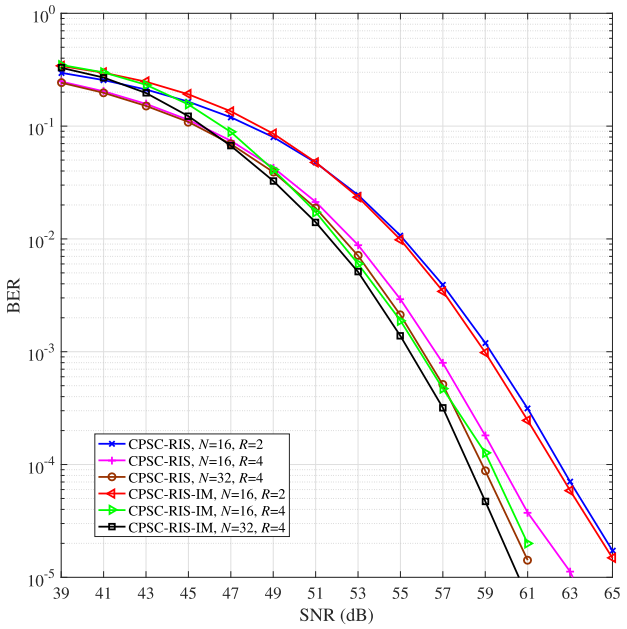

Fig. 8. Performance comparison between CPSC-RIS and CPSC-RIS-IM with $N = 16, 32, M = 2, R = 2, 4$, and perfect CSI at the receiver.

CPSC-RIS with $R = 4$ obtains about 3 dB SNR gain over that with $R = 2$, at a BER value of 10^{-4}. Increasing the value of N achieves SNR gains of 2 dB and 1 dB for CPSC-RIS and CPSC, respectively, at a BER value of 10^{-4}. By contrast, a larger constellation size deteriorates the performance (about 2 dB SNR loss) for both CPSC-RIS and CPSC.

Fig. 7 presents the performance comparison between CPSC-RIS and CPSC with perfect and estimated CSI at the receiver, where $N = 16, 32, M = 2$, and $R = 6$. The estimated CSI is obtained via (11). As expected, all schemes with estimated CSI perform worse than the corresponding schemes with perfect CSI, and approximately 4 dB SNR loss is incurred by the imperfect CSI. We observe from Fig. 7 that, in both cases, increasing the value of N from 16 to 32 leads to SNR gains for both CPSC-RIS and CPSC. Specifically, the SNR gain for CPSC-RIS is about 1 dB at a BER value of 10^{-4}, while that for CPSC is minor. With both perfect and estimated CSI at the receiver, CPSC-RIS outperforms CPSC for all considered SNR values. Moreover, for $N = 16$ and 32, CPSC-RIS with estimated CSI achieves about 7 dB and 8 dB SNR gains, respectively, over CPSC with perfect CSI, at a BER value of 10^{-4}.

In Fig. 8, we compare the BER performance of CPSC-RIS and CPSC-RIS-IM, where $N = 16, 32, M = 2, R = 2, 4$, and perfect CSI is assumed at the receiver. As seen from Fig. 8, CPSC-RIS-IM outperforms CPSC-RIS at high SNR with the same parameter settings. Particularly, the performance gain achieved by CPSC-RIS-IM over CPSC-RIS for $R = 4$ is larger than that for $R = 2$. This can be explained as follows. The cyclic delay constraints in Section II are met for both $R = 2$ and $R = 4$. As seen from (8), increasing the value of R from 2 to 4 enhances the equivalent CIR. Hence, the performance of both CPSC-RIS-IM and CPSC-RIS becomes better when R increases from 2 to 4. Moreover, for CPSC-RIS-IM, a larger value of R results in more transmitted IM

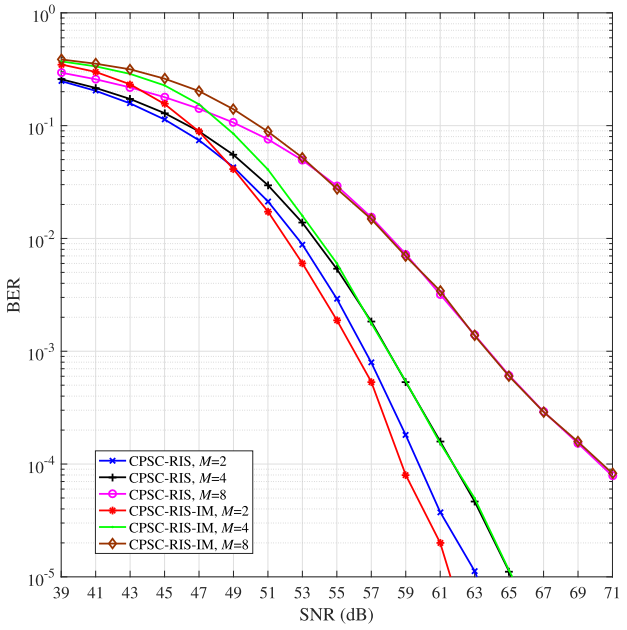

Fig. 9. Performance comparison between CPSC-RIS and CPSC-RIS-IM with $N = 16, R = 4, M = 2, 4, 8$, and perfect CSI at the receiver.

bits, and the transmit power becomes higher for a given value of SNR=E_b/N_0. In addition, the transmission of IM bits itself does not consume power. Therefore, the performance improvement for CPSC-RIS-IM is more significant than that for CPSC-RIS when R increases from 2 to 4. Also, increasing the value of N enhances the performance of both CPSC-RIS and CPSC-RIS-IM. In particular, doubling the value of R has a more significant impact than that of N on both CPSC-RIS and CPSC-RIS-IM. Specifically, about 3 dB and 1 dB SNR gains can be achieved at a BER value of 10^{-4}, by increasing

the value of R from 2 to 4 and the value of N from 16 to 32, respectively.

Fig. 9 illustrates the performance comparison between CPSC-RIS and CPSC-RIS-IM, where $N = 16, R = 4, M = 2, 4, 8$, and perfect CSI is assumed at the receiver. As shown in Fig. 9, with $M = 2$, CPSC-RIS-IM performs better than CPSC-RIS for practical BER values with SNR$>$ 49 dB. With increasing the value of M, the superiority of CPSC-RIS-IM over CPSC-RIS is lost. This is because that the proportion of the IM bits in CPSC-RIS-IM decreases with increasing the value of M. However, from Fig. 6, it is expected that CPSC-RIS-IM still achieves much better BER performance than conventional CPSC without RIS and CDD.

VI. Conclusion

In this paper, we have proposed a CDD-enhancing CPSC transmission scheme for RIS-aided broadband wireless systems. The channel estimation, signal detection, and SE improvement have all been studied for CPSC-RIS. Specifically, a practical and efficient time-domain channel estimator has been developed for CPSC-RIS, which can be considered as a general channel estimator for RIS-aided broadband communications. The optimal ML and low-complexity ZF/MMSE detectors have been designed for CPSC-RIS, and the BER performance of the ML detector over frequency-selective Nakagami-m fading channels has been analyzed with the theoretically derived upper bound. Further, CPSC-RIS has been extended to CPSC-RIS-IM for improving the SE by using the concept of IM. We conclude that the proposed two schemes can be considered as promising candidates for RIS-empowered broadband wireless communications.

Appendix A
Proof of Proposition 1

Since $\mathbf{X}_p$ is a circulant matrix, $\mathbf{X}_p^H\mathbf{X}_p$ is also a circulant matrix and can be expressed as $\mathbf{X}_p^H\mathbf{X}_p = \mathrm{cir}(\mathbf{x}_{pp})$, where $\mathbf{x}_{pp} = [x_{pp}(1), x_{pp}(2), \ldots, x_{pp}(N)]^T$ with $x_{pp}(n) = \mathbf{x}_p^H(n-1)\mathbf{x}_p$ and $\mathbf{x}_p(n-1)$ being the cyclically delayed version of $\mathbf{x}_p$ with the cyclic delay $n-1$ for $n = 1, \ldots, N$. Obviously, we have $x_{pp}(1) = \mathbf{x}_p^H\mathbf{x}_p = N$.

Further, as a circulant matrix, $\mathbf{X}_p^H\mathbf{X}_p$ can be decomposed as $\mathbf{X}_p^H\mathbf{X}_p = \mathbf{F}^{-1}\mathbf{D}\mathbf{F}$, where $\mathbf{F}$ is the unitary DFT matrix and $\mathbf{D}_p = \mathrm{diag}([d_p(1), \ldots, d_p(N)]^T)$ with

$$d_p(k) = \sum_{n=1}^{N} x_{pp}(n) \exp\left(-j\frac{2\pi(n-1)(k-1)}{N}\right) \quad (39)$$

and $\sum_{k=1}^{N} d_p(k) = \mathrm{Tr}\left\{\mathbf{X}_p^H\mathbf{X}_p\right\} = N^2$. From (12), the MSE can be rewritten as

$$\begin{aligned}\epsilon &= N_0\mathrm{Tr}\left\{\left(\mathbf{X}_p^H\mathbf{X}_p\right)^{-1}\right\} = N_0\mathrm{Tr}\left\{\mathbf{F}^{-1}\mathbf{D}_p^{-1}\mathbf{F}\right\} \\ &= N_0\mathrm{Tr}\left\{\mathbf{D}_p^{-1}\right\} = N_0\sum_{k=1}^{N}\frac{1}{d_p(k)}. \end{aligned} \quad (40)$$

From (40), under the condition that $\sum_{k=1}^{N} d_p(k) = N^2$, to minimize the MSE, we should have $d_p(1) = \ldots = d_p(N) = N$. Finally, we conclude that $x_{pp} = [N, 0, \ldots, 0]^T$ and $\mathbf{X}_p^H\mathbf{X}_p = N\mathbf{I}_{N\times N}$ when the MSE is minimized, which completes the proof.

References

[1] Q. Li, M. Wen, E. Basar, G. C. Alexandropoulos, K. J. Kim, and H. V. Poor, "Cyclic-prefixed single-carrier transmission with reconfigurable intelligent surfaces," in *Proc. Joint Eur. Conf. Netw. Commun. 6G Summit (EuCNC/6G Summit)*, Grenoble, France, Jun. 2022, pp. 512–517.

[2] F. Pancaldi, G. M. Vitetta, R. Kalbasi, N. Al-Dhahir, M. Uysal, and H. Mheidat, "Single-carrier frequency domain equalization," *IEEE Signal Process. Mag.*, vol. 25, no. 5, pp. 37–56, Sep. 2008.

[3] D. Falconer, S. L. Ariyavisitakul, A. Benyamin-Seeyar, and B. Eidson, "Frequency domain equalization for single-carrier broadband wireless systems," *IEEE Commun. Mag.*, vol. 40, no. 4, pp. 58–66, Apr. 2002.

[4] B. Devillers, J. Louveaux, and L. Vandendorpe, "About the diversity in cyclic prefixed single-carrier systems," *Phys. Commun.*, vol. 1, no. 4, pp. 266–276, Dec. 2008.

[5] K. J. Kim and T. A. Tsiftsis, "Performance analysis of QRD-based cyclically prefixed single-carrier transmissions with opportunistic scheduling," *IEEE Trans. Veh. Technol.*, vol. 60, no. 1, pp. 328–333, Jan. 2011.

[6] K. J. Kim, H. Liu, Z. Ding, P. V. Orlik, and H. V. Poor, "Diversity gain analysis of distributed CDD systems in non-identical fading channels," *IEEE Trans. Commun.*, vol. 68, no. 11, pp. 7218–7231, Nov. 2020.

[7] A. Dammann and S. Kaiser, "Standard conformable antenna diversity techniques for OFDM and its application to the DVB-T system," in *Proc. IEEE Global Telecommun. Conf. (GLOBECOM)*, San Antonio, TX, USA, Nov. 2001, pp. 388–397.

[8] U. K. Kwon and G. H. Im, "Cyclic delay diversity with frequency domain turbo equalization for uplink fast fading channels," *IEEE Commun. Lett.*, vol. 13, no. 3, pp. 184–186, Mar. 2009.

[9] Y.-C. Liang, W. S. Leon, Y. Zeng, and C. Xu, "Design of cyclic delay diversity for single carrier cyclic prefix (SCCP) transmissions with block-iterative GDFE (BI-GDFE) receiver," *IEEE Trans. Wireless Commun.*, vol. 7, no. 2, pp. 677–684, Feb. 2008.

[10] K. J. Kim, M. Di Renzo, H. Liu, P. V. Orlik, and H. V. Poor, "Performance analysis of distributed single carrier systems with distributed cyclic delay diversity," *IEEE Trans. Commun.*, vol. 65, no. 12, pp. 5514–5528, Dec. 2017.

[11] K. J. Kim, H. Liu, M. Wen, P. V. Orlik, and H. V. Poor, "Secrecy performance analysis of distributed asynchronous cyclic delay diversity-based cooperative single carrier systems," *IEEE Trans. Commun.*, vol. 68, no. 5, pp. 2680–2694, May 2020.

[12] N. Iradukunda, H. T. Nguyen, and W.-J. Hwang, "On cyclic delay diversity-based single-carrier scheme in spectrum sharing systems," *IEEE Commun. Lett.*, vol. 23, no. 6, pp. 1069–1072, Jun. 2019.

[13] E. Basar, M. Di Renzo, J. De Rosny, M. Debbah, M. Alouini, and R. Zhang, "Wireless communications through reconfigurable intelligent surfaces," *IEEE Access*, vol. 7, pp. 116753–116773, 2019.

[14] M. Di Renzo et al., "Smart radio environments empowered by reconfigurable AI meta-surfaces: An idea whose time has come," *EURASIP J. Wireless Commun. Netw.*, vol. 2019, no. 1, pp. 1–20, May 2019.

[15] M. Jian et al., "Reconfigurable intelligent surfaces for wireless communications: Overview of hardware designs, channel models, and estimation techniques," *Intell. Converged Netw.*, vol. 3, no. 1, pp. 1–32, Mar. 2022.

[16] E. Calvanese Strinati et al., "Reconfigurable, intelligent, and sustainable wireless environments for 6G smart connectivity," *IEEE Commun. Mag.*, vol. 59, no. 10, pp. 99–105, Oct. 2021.

[17] C. Huang, A. Zappone, G. C. Alexandropoulos, M. Debbah, and C. Yuen, "Reconfigurable intelligent surfaces for energy efficiency in wireless communication," *IEEE Trans. Wireless Commun.*, vol. 18, no. 8, pp. 4157–4170, Aug. 2019.

[18] Q. Wu and R. Zhang, "Intelligent reflecting surface enhanced wireless network via joint active and passive beamforming," *IEEE Trans. Wireless Commun.*, vol. 18, no. 11, pp. 5394–5409, Nov. 2019.

[19] H. Guo, Y.-C. Liang, J. Chen, and E. G. Larsson, "Weighted sum-rate maximization for reconfigurable intelligent surface aided wireless networks," *IEEE Trans. Wireless Commun.*, vol. 19, no. 5, pp. 3064–3076, May 2020.

[20] S. Hong, C. Pan, H. Ren, K. Wang, K. K. Chai, and A. Nallanathan, "Robust transmission design for intelligent reflecting surface-aided secure communication systems with imperfect cascaded CSI," *IEEE Trans. Wireless Commun.*, vol. 20, no. 4, pp. 2487–2501, Apr. 2021.

[21] L. Du, C. Huang, W. Guo, J. Ma, X. Ma, and Y. Tang, "Reconfigurable intelligent surfaces assisted secure multicast communications," *IEEE Wireless Commun. Lett.*, vol. 9, no. 10, pp. 1673–1676, Oct. 2020.

[22] G. C. Alexandropoulos, K. Katsanos, M. Wen, and D. B. Da Costa, "Safeguarding MIMO communications with reconfigurable metasurfaces and artificial noise," in *Proc. IEEE Int. Conf. Commun. (ICC)*, Montreal, QC, Canada, Jun. 2021, pp. 1–6.
[23] I. Yildirim, F. Kilinc, E. Basar, and G. C. Alexandropoulos, "Hybrid RIS-empowered reflection and decode-and-forward relaying for coverage extension," *IEEE Commun. Lett.*, vol. 25, no. 5, pp. 1692–1696, May 2021.
[24] J. Ye, S. Guo, and M.-S. Alouini, "Joint reflecting and precoding designs for SER minimization in reconfigurable intelligent surfaces assisted MIMO systems," *IEEE Trans. Wireless Commun.*, vol. 19, no. 8, pp. 5561–5574, Aug. 2020.
[25] Z. Abu-Shaban, K. Keykhosravi, M. F. Keskin, G. C. Alexandropoulos, G. Seco-Granados, and H. Wymeersch, "Near-field localization with a reconfigurable intelligent surface acting as lens," in *Proc. IEEE Int. Conf. Commun.*, Jun. 2021, pp. 1–6.
[26] W. Tang et al., "MIMO transmission through reconfigurable intelligent surface: System design, analysis, and implementation," *IEEE J. Sel. Areas Commun.*, vol. 38, no. 11, pp. 2683–2699, Nov. 2020.
[27] W. Tang et al., "Realization of reconfigurable intelligent surface-based Alamouti space-time transmission," in *Proc. Int. Conf. Wireless Commun. Signal Process. (WCSP)*, Nanjing, China, Oct. 2020, pp. 904–909.
[28] E. Basar, "Index modulation techniques for 5G wireless networks," *IEEE Commun. Mag.*, vol. 54, no. 7, pp. 168–175, Jul. 2016.
[29] A. E. Canbilen, E. Basar, and S. S. Ikki, "Reconfigurable intelligent surface-assisted space shift keying," *IEEE Wireless Commun. Lett.*, vol. 9, no. 9, pp. 1495–1499, Sep. 2020.
[30] Q. Li, M. Wen, S. Wang, G. C. Alexandropoulos, and Y.-C. Wu, "Space shift keying with reconfigurable intelligent surfaces: Phase configuration designs and performance analysis," *IEEE Open J. Commun. Soc.*, vol. 2, pp. 322–333, 2021.
[31] S. Luo et al., "Spatial modulation for RIS-assisted uplink communication: Joint power allocation and passive beamforming design," *IEEE Trans. Commun.*, vol. 69, no. 10, pp. 7017–7031, Oct. 2021.
[32] Q. Li, M. Wen, and M. Di Renzo, "Single-RF MIMO: From spatial modulation to metasurface-based modulation," *IEEE Wireless Commun.*, vol. 28, no. 4, pp. 88–95, Aug. 2021.
[33] S. Guo, S. Lv, H. Zhang, J. Ye, and P. Zhang, "Reflecting modulation," *IEEE J. Sel. Areas Commun.*, vol. 38, no. 11, pp. 2548–2561, Nov. 2020.
[34] W. Yan, X. Yuan, Z.-Q. He, and X. Kuai, "Passive beamforming and information transfer design for reconfigurable intelligent surfaces aided multiuser MIMO systems," *IEEE J. Sel. Areas Commun.*, vol. 38, no. 8, pp. 1793–1808, Aug. 2020.
[35] E. Basar, "Reconfigurable intelligent surface-based index modulation: A new beyond MIMO paradigm for 6G," *IEEE Trans. Commun.*, vol. 68, no. 5, pp. 3187–3196, May 2020.
[36] S. P. Dash, R. K. Mallik, and N. Pandey, "Performance analysis of an index modulation-based receive diversity RIS-assisted wireless communication system," *IEEE Commun. Lett.*, vol. 26, no. 4, pp. 768–772, Apr. 2022.
[37] J. Yuan, M. Wen, Q. Li, E. Basar, G. C. Alexandropoulos, and G. Chen, "Receive quadrature reflecting modulation for RIS-empowered wireless communications," *IEEE Trans. Veh. Technol.*, vol. 70, no. 5, pp. 5121–5125, May 2021.
[38] S. Gopi, S. Kalyani, and L. Hanzo, "Intelligent reflecting surface assisted beam index-modulation for millimeter wave communication," *IEEE Trans. Wireless Commun.*, vol. 20, no. 2, pp. 983–996, Feb. 2021.
[39] S. Lin, B. Zheng, G. C. Alexandropoulos, M. Wen, M. Di Renzo, and F. Chen, "Reconfigurable intelligent surfaces with reflection pattern modulation: Beamforming design and performance analysis," *IEEE Trans. Wireless Commun.*, vol. 20, no. 2, pp. 741–754, Feb. 2021.
[40] S. Lin, F. Chen, M. Wen, Y. Feng, and M. Di Renzo, "Reconfigurable intelligent surface-aided quadrature reflection modulation for simultaneous passive beamforming and information transfer," *IEEE Trans. Wireless Commun.*, vol. 21, no. 3, pp. 1469–1481, Mar. 2022.
[41] Y. Yang, B. Zheng, S. Zhang, and R. Zhang, "Intelligent reflecting surface meets OFDM: Protocol design and rate maximization," *IEEE Trans. Commun.*, vol. 68, no. 7, pp. 4522–4535, Mar. 2020.
[42] B. Zheng and R. Zhang, "Intelligent reflecting surface-enhanced OFDM: Channel estimation and reflection optimization," *IEEE Wireless Commun. Lett.*, vol. 9, no. 4, pp. 518–522, Apr. 2020.
[43] S. Lin, B. Zheng, G. C. Alexandropoulos, M. Wen, F. Chen, and S. Mumtaz, "Adaptive transmission for reconfigurable intelligent surface-assisted OFDM wireless communications," *IEEE J. Sel. Areas Commun.*, vol. 38, no. 11, pp. 2653–2665, Nov. 2020.
[44] G. C. Alexandropoulos, S. Samarakoon, M. Bennis, and M. Debbah, "Phase configuration learning in wireless networks with multiple reconfigurable intelligent surfaces," in *Proc. IEEE Globecom Workshops (GC Wkshps*, Taiwan, Dec. 2020, pp. 1–6.
[45] S. P. Dash, R. K. Mallik, and S. K. Mohammed, "Coherent detection in a receive diversity PLC system under Nakagami-m noise environment," in *Proc. 27th Annu. IEEE Int. Symp. Per., Indoor, Mobile Radio Commun. (PIMRC)*, Valencia, Spain, Sep. 2016, pp. 1–6.
[46] R. K. Mallik, "A new statistical model of the complex Nakagami-m fading gain," *IEEE Trans. Commun.*, vol. 58, no. 9, pp. 2611–2620, Sep. 2010.
[47] G. C. Alexandropoulos, P. T. Mathiopoulos, and N. C. Sagias, "Switch-and-examine diversity over arbitrary correlated Nakagami-m fading channels," *IEEE Trans. Veh. Technol.*, vol. 59, no. 4, pp. 2080–2087, May 2010.
[48] D. Chu, "Polyphase codes with good periodic correlation properties," *IEEE Trans. Inf. Theory*, vol. IT-18, no. 4, pp. 531–532, Jul. 1972.
[49] T. L. Jensen and E. De Carvalho, "An optimal channel estimation scheme for intelligent reflecting surfaces based on a minimum variance unbiased estimator," in *Proc. IEEE Int. Conf. Acoust., Speech Signal Process. (ICASSP)*, Barcelona, Spain, May 2020, pp. 5000–5004.
[50] M. Chiani, D. Dardari, and M. K. Simon, "New exponential bounds and approximations for the computation of error probability in fading channels," *IEEE Trans. Wireless Commun.*, vol. 2, no. 4, pp. 840–845, Jul. 2003.
[51] M. Wen, S. Lin, K. J. Kim, and F. Ji, "Cyclic delay diversity with index modulation for green Internet of Things," *IEEE Trans. Green Commun. Netw.*, vol. 5, no. 2, pp. 600–610, Jun. 2021.
[52] M. Wen, E. Basar, Q. Li, B. Zheng, and M. Zhang, "Multiple-mode orthogonal frequency division multiplexing with index modulation," *IEEE Trans. Commun.*, vol. 65, no. 9, pp. 3892–3906, Sep. 2017.
[53] Z. Zhang et al., "Active RIS vs. passive RIS: Which will prevail in 6G?" 2021, *arXiv:2103.15154*.

Qiang Li (Member, IEEE) received the Ph.D. degree from the South China University of Technology, Guangzhou, China, in 2020. From 2018 to 2019, he was a Visiting Student Research Collaborator at Princeton University, Princeton, NJ, USA. Since 2020, he has been an Assistant Professor with Jinan University, Guangzhou. His current research interests include index modulation and reconfigurable intelligent surfaces. He was a recipient of the Excellent Doctoral Dissertation Award from the China Education Society of Electronics, and the Best Paper Award from the IEEE International Conference on Communication Technology in 2019. He is currently serving as an Editor for the IEEE COMMUNICATIONS LETTERS.

Miaowen Wen (Senior Member, IEEE) received the Ph.D. degree from Peking University, Beijing, China, in 2014.

From 2019 to 2021, he was at the Department of Electrical and Electronic Engineering, The University of Hong Kong, Hong Kong, as a Post-Doctoral Research Fellow. He is currently a Professor with the South China University of Technology, Guangzhou, China. He has published two books and more than 170 journal articles. His research interests include a variety of topics in the areas of wireless and molecular communications. He was a recipient of the IEEE ComSoc Asia-Pacific Outstanding Young Researcher Award in 2020 and five Best Paper Awards from the IEEE ITST'12, the IEEE ITSC'14, the IEEE ICNC'16, the IEEE ICCT'19, and the EAI QSHINE'22. He was the Winner in Data Bakeoff Competition (Molecular MIMO) from the 2019 IEEE Communication Theory Workshop (CTW), Selfoss, Iceland. He served as a Guest Editor for the IEEE JOURNAL ON SELECTED AREAS IN COMMUNICATIONS and the IEEE JOURNAL OF SELECTED TOPICS IN SIGNAL PROCESSING. He is currently serving as an Editor for the IEEE TRANSACTIONS ON COMMUNICATIONS, the IEEE TRANSACTIONS ON MOLECULAR, BIOLOGICAL, AND MULTI-SCALE COMMUNICATIONS, and the IEEE COMMUNICATIONS LETTERS.

Ertugrul Basar (Fellow, IEEE) received the Ph.D. degree from Istanbul Technical University in 2013. He is currently an Associate Professor with the Department of Electrical and Electronics Engineering, Koç University, İstanbul, Turkey, and the Director of the Communications Research and Innovation Laboratory (CoreLab). In the past, he had visiting positions at Ruhr University Bochum, Germany (2022, Mercator Fellow), and Princeton University, USA (2011–2012, Visiting Research Collaborator). His primary research interests include beyond 5G and 6G wireless networks, communication theory and systems, reconfigurable intelligent surfaces, index modulation, waveform design, and signal processing for communications. He has been a Young Member of Turkish Academy of Sciences since 2017. He served as an Editor/Senior Editor for many journals including IEEE COMMUNICATIONS LETTERS (2016–2022), IEEE TRANSACTIONS ON COMMUNICATIONS (2018–2022), *Physical Communication* (2017–2020), and IEEE ACCESS (2016–2018). He is currently an Editor of *Frontiers in Communications and Networks*.

George C. Alexandropoulos (Senior Member, IEEE) received the Engineering Diploma, M.A.Sc., and Ph.D. degrees in computer engineering and informatics from the School of Engineering, University of Patras, Greece, in 2003, 2005, and 2010, respectively. He has held research positions at various Greek universities and research institutes, as well as at the Mathematical and Algorithmic Sciences Laboratory, Paris Research Center, Huawei Technologies France. He is currently an Assistant Professor with the Department of Informatics and Telecommunications, School of Sciences, National and Kapodistrian University of Athens (NKUA), Greece. He also serves as a Principal Researcher for the Technology Innovation Institute, Abu Dhabi, United Arab Emirates. His research interests span the general areas of algorithmic design and performance analysis for wireless networks with emphasis on multi-antenna transceiver hardware architectures, active and passive reconfigurable intelligent surfaces (RISs), integrated communications and sensing, full duplex radios, millimeter wave, and THz communications, as well as distributed machine learning algorithms. He is a Senior Member of the IEEE Communications, Signal Processing, Vehicular Technology, and Information Theory Societies, the Vice-Chair of the EURASIP Technical Area Committee on Signal Processing for Communications and Networking, as well as a registered Professional Engineer of the Technical Chamber of Greece. He is also a Distinguished Lecturer of the IEEE Communications Society. He has participated and/or technically managed more than 15 European Union (EU), international, and Greek research, innovation, and development projects. He is currently NKUA's Principal Investigator for the EU H2020 RISE-6G and the SNS JU TERRAMETA projects dealing with RIS-empowered smart wireless environments and THz RISs, respectively. For the former project, he also serves as the Dissemination Manager, whereas for the latter, he also serves as the Project's Technical Manager. He has received the Best Ph.D. Thesis Award 2010, the IEEE Communications Society Best Young Professional in Industry Award 2018, the EURASIP Best Paper Award of the Journal on Wireless Communications and Networking 2021, the IEEE Marconi Prize Paper Award in Wireless Communications 2021, and a Best Paper Award from the IEEE GLOBECOM 2021. In the past, he has held various fixed-term and guest editorial positions for IEEE TRANSACTIONS ON WIRELESS COMMUNICATIONS and IEEE COMMUNICATIONS LETTERS, as well as for various special issues at IEEE journals. He currently serves as an Editor for IEEE TRANSACTIONS ON COMMUNICATIONS, IEEE WIRELESS COMMUNICATIONS LETTERS, *Computer Networks* (Elsevier), *Frontiers in Communications and Networks*, and the *ITU Journal on Future and Evolving Technologies*. More information is available at www.alexandropoulos.info.

Kyeong Jin Kim (Senior Member, IEEE) received the M.S. degree from the Korea Advanced Institute of Science and Technology (KAIST) in 1991 and the M.S. and Ph.D. degrees in electrical and computer engineering from the University of California, Santa Barbara, CA, USA, in 2000. From 1991 to 1995, he was a Research Engineer at the Video Research Center, Daewoo Electronics, Ltd., South Korea. In 1997, he joined the Data Transmission and Networking Laboratory, University of California, Santa Barbara. After receiving his degrees, he joined the Nokia Research Center and Nokia Inc., Dallas, TX, USA, as a Senior Research Engineer, where he was an L1 Specialist, from 2005 to 2009. From 2010 to 2011, he was a Visiting Scholar at Inha University, South Korea. Since 2012, he has been a Senior Principal Research Staff with the Mitsubishi Electric Research Laboratories, Cambridge, MA, USA. His research includes transceiver design, resource management, scheduling in the cooperative wireless communications system, cooperative spectrum sharing system, physical layer secrecy system, device-to-device communications, local and private 5G networks, and AI-based smart grid systems.

He served as an Editor for IEEE COMMUNICATIONS LETTERS and IEEE TRANSACTIONS ON COMMUNICATIONS, a Guest Editor for the *IET Communications* Special Issue on Secure Physical Layer Communications, a leading Guest Editor for the IEEE JOURNAL ON SELECTED AREAS IN COMMUNICATIONS Special issue on Spatial Modulation for Emerging Wireless Systems, and a leading Guest Editor for the IEEE JOURNAL OF SELECTED TOPICS IN SIGNAL PROCESSING Special issue on Advanced Signal Processing for Local and Private 5G Networks. He received the Best Paper Award in 2014 IEEE-Chinacom, IEEE ICC-2019, and IEEE PES-GM 2020.

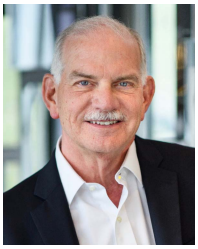

H. Vincent Poor (Life Fellow, IEEE) received the Ph.D. degree in EECS from Princeton University in 1977. From 1977 to 1990, he was on the faculty of the University of Illinois at Urbana-Champaign. Since 1990, he has been on the faculty at Princeton, where he is currently the Michael Henry Strater University Professor. From 2006 to 2016, he served as the Dean of Princeton's School of Engineering and Applied Science. He has also held visiting appointments at several other universities, including most recently at Berkeley and Cambridge. His research interests are in the areas of information theory, machine learning and network science, and their applications in wireless networks, energy systems, and related fields. Among his publications in these areas is the recent book *Machine Learning and Wireless Communications* (Cambridge University Press, 2022). He is a member of the National Academy of Engineering and the National Academy of Sciences and a foreign member of the Chinese Academy of Sciences, the Royal Society, and other national and international academies. He received the IEEE Alexander Graham Bell Medal in 2017.